

99 new oscillating red-giant stars in binary systems with NASA TESS and NASA *Kepler* identified from the SB9-Catalogue

P. G. Beck^{1,2}, S. Mathur^{2,3}, K. Hambleton⁴, R. A. García⁵, L. Steinwender¹,
N. L. Eisner⁶, J.-D. do Nascimento^{7,8}, P. Gaulme⁹, and S. Mathis⁵

¹ Institut für Physik, Karl-Franzens Universität Graz, Universitätsplatz 5/II, NAWI Graz, 8010 Graz, Austria .
e-mail: paul.beck@uni-graz.at

² Instituto de Astrofísica de Canarias, E-38200 La Laguna, Tenerife, Spain

³ Departamento de Astrofísica, Universidad de La Laguna, E-38206 La Laguna, Tenerife, Spain

⁴ Department of Astrophysics and Planetary Science, Villanova University, 800 East Lancaster Avenue, Villanova, PA 19085, USA

⁵ AIM, CEA, CNRS, Université de Paris F-91191 Gif-sur-Yvette, France

⁶ Department of Physics, University of Oxford, Keble Road, Oxford OX1 3RH, UK

⁷ Center for Astrophysics, Harvard & Smithsonian, 60 Garden Street, Cambridge, MA 02138, USA

⁸ Departamento de Física, Universidade Federal do Rio Grande do Norte, CEP: 59072-970 Natal, RN, Brazil

⁹ Max-Planck-Institut für Sonnensystemforschung, Justus-von-Liebig-Weg 3, 37077 Göttingen, Germany

Version of February 8, 2022

ABSTRACT

Oscillating red-giant stars in binary systems are an ideal testbed for investigating the structure and evolution of stars in the advanced phases of evolution. With 83 known red-giants in binary systems, of which only ~40 have determined global seismic parameters and orbital parameters, the sample is slender compared to the numerous known oscillating stars. The detection of red-giant binary systems is typically obtained from the signature of stellar binarity in space photometry. The time base of such data biases the detection towards systems with shorter periods and orbits of insufficient size to allow a red-giant to fully extend as it evolves up the red-giant branch. Consequently, the sample shows an excess of H-shell burning giants while being sparse of stars in the He-core burning phase. From the *ninth catalogue of spectroscopic binary orbits* (SB9), we identified candidate systems hosting a red-giant primary component. Searching space photometry from the NASA missions *Kepler*, K2, and TESS (*Transiting Exoplanet Survey Satellite*) as well as the BRITe (*BR*ight *T*arget *E*xplorer) constellation mission, we found 99 systems, which were previously unknown of hosting an oscillating giant component. The revised search strategy allowed us to extend the range of orbital periods of systems hosting oscillating giants up to 26 000 days. Such wide orbits allow for a rich population of He-core burning primaries, which are required for a complete view on stellar evolution from binary studies. Tripling the size of known oscillating red-giant stars in binary systems is an important step towards an ensemble approach for seismology and tidal studies. While for non-eclipsing binaries the inclination is unknown, such a seismically well-characterized sample will be a treasure trove in combination with *Gaia* astrometric orbits for binary systems.

Key words. Asteroseismology – (Stars:) binaries: spectroscopic – Stars: late-type – Stars: oscillations (including pulsations).

1. Introduction

Binary systems are gravitationally-bound pairs of stars that orbit around a common center of mass (e.g. Prša 2018). Unless created in a rare capturing event, both stellar components are born from the same cloud. Because both stars are located at the same distance and have similar initial conditions and stellar age, we are able to place significant constraints on input parameters for the stellar models. Studying such well-constrained systems offers the opportunity to test complex microscopic and macroscopic physics through stellar models (e.g. Johnston et al. 2019).

If a stellar component is oscillating then asteroseismology (Christensen-Dalsgaard 1984) the characterization of the internal structure and dynamics of stars through oscillation modes, can provide independently inferred crucial information on the stellar mass, radius and age of the oscillating components (see monograph of Aerts, Christensen-Dalsgaard, & Kurtz 2010, and references therein). Binary systems that host solar-like oscillators are of particular interest. Stochastic oscillations driven through convection are found in many objects from solar-like

dwarfs to luminous red-giant stars and allow the investigation of a wide range of stellar evolutionary phases with a consistent methodology.

Despite the large number of more than 16 000 known solar-like oscillating red-giant (RG) stars (Yu et al. 2018) from the NASA *Kepler* spacecraft (Borucki et al. 2010) alone, there are only 83 known red-giant oscillators in binary systems. This sample was compiled from the analysis of photometric data in a series of papers summarized and referenced in Tables A.1, A.2, and A.3. Studying these systems led to exciting insights into the evolution of evolved stars, such as the effect of structural changes on the seismic scaling relations (Gaulme et al. 2016; Themeßl et al. 2018; Kallinger et al. 2018; Benbakoura et al. 2021), studies of tides (Beck et al. 2018b), surface rotation and activity (Gaulme et al. 2014) or the seismic probing of the first dredge-up event and internal rotational gradient (Beck et al. 2018a).

About 3000 binary stars have been identified in the *Kepler* data (Prša et al. 2011; Kirk et al. 2016). The majority of these stars are oriented such that the orbital plane is edge-on and

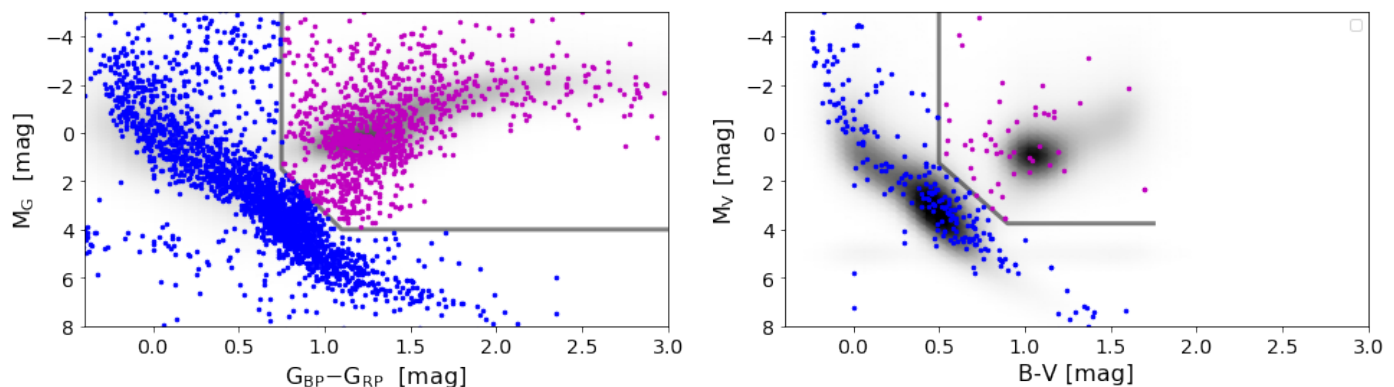


Fig. 1. Color-magnitude diagrams depicting the position of the systems listed in the SB9 catalogue using *Gaia* DR2 (left) and *Hipparcos* astrometry (right panel). Magenta dots indicate candidates of hosting primaries in advanced phases of stellar evolution. Blue dots mark the remaining systems. The grey line indicates the selection criterion for red-giant candidates. The background density plots represent the distribution of all stars measured by the respective mission, with a limiting magnitude in V of 10 mag.

eclipses occur; however, many of these (~ 800 in the *Kepler* data) present ellipsoidal variations. The majority of ellipsoidal systems have close-to-zero eccentricity due to their small orbits although 117 of the *Kepler* sample are eccentric and colloquially referred to as *heartbeat stars*, a term coined by Thompson et al. (2012) due to the shape of the light curve (Kumar et al. 1995). Longer-period non-eclipsing systems, however, of moderate eccentricity are hardly found from time-series photometry. A similar problem exists for eclipsing systems if the orbital periods exceed the timeseries’s timebase. Binary systems detected from eclipses observed with space-photometric data are biased towards relatively short orbital periods. For a mission like *Kepler*, with a time base of 4 yr the majority of the sample extends up to 2-3 yr. Longer-periodic systems are normally discovered through radial-velocity (RV) variations from spectroscopic surveys (e.g. Badenes et al. 2018). Coordinated and long-term RV monitoring is then required to determine their orbital parameters. The *ninth catalogue of spectroscopic binary orbits*¹ (SB9) by Pourbaix et al. (2004) provides a compilation of 4004 solved orbits of binary and triple systems across all spectral types and a wide range of orbital periods.

This paper is structured as follows. In Sec. 2 we use the SB9 catalog to search for known binaries, which potentially host a red-giant primary. Section 3 describes our search of existing space-photometry data of the NASA *Kepler*, its refurbished K2 missions (Howell et al. 2014), the BRITe (*BRIght Target Explorer*) constellation space telescopes (Weiss et al. 2014), and the ongoing all-sky survey with *Transiting Exoplanet Survey Satellite*, TESS (Ricker et al. 2014) for unknown oscillating red-giant stars in these systems. The seismic analysis of the newly found systems, containign an oscillating red-giant component is explained in Sec. 4. In Sec. 5 and 6 we discuss the the seismic and orbital parameters of the result of this work to the sample in the literature. The work is summarized in Sec. 7.

2. Identifying red giants in SB9

Systems in the SB9 catalog are typically brighter than 12th magnitude. Pourbaix et al. (2004) note that the collection is rich in stars of spectral types later than mid-F, which are the spectral classes where solar-like oscillations are expected. First results on red giants from the TESS mission by Silva Aguirre et al. (2020),

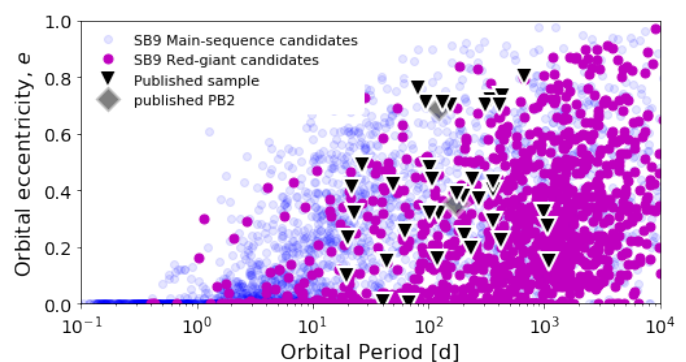


Fig. 2. Position of the SB9 binary systems (Pourbaix et al. 2004) in the e-P plane. Magenta and blue dots indicate all systems found through the photometric calibration described in Sec. 2 and Fig. 1 to host a primary in an advanced stellar evolutionary phase and on the main sequence, respectively. Systems from the published *Kepler* sample with an oscillating red-giant primary are depicted as black triangles. Systems hosting two oscillating red-giant components (PB2) are shown as gray diamonds.

Mackereth et al. (2021) and ? show that this magnitude range is well-suited for detecting red-giant oscillations with the satellite.

The search for oscillating red-giant stars in binary systems started with a photometric calibration of the SB9 catalog. Stars in advanced evolutionary phases were identified through their position on a color-magnitude diagram (CMD). For the majority of the systems in the SB9 catalog, astrometric solutions and multi-color photometry are available in the *Gaia* data release 2 (Gaia Collaboration et al. 2018, DR2). We therefore use the $G_{BP}-G_{RP}$ color index as a temperature proxy. The provided *Gaia* distance module allows us to calculate the absolute visual magnitude, M_G (Fig. 1, left panel). For about 230 SB9-systems, no *Gaia* solution exists in DR2, but parallaxes were measured by the ESA *Hipparcos* mission (van Leeuwen 2007). For these systems, the classical Johnson B-V color index was used, and the absolute magnitude was calculated for Johnson V (Fig. 1, right panel).

To guide the reader’s eye in the respective parameter space in Fig. 1, the density distributions of stars brighter than 10th magnitude are shown in the background of the CMD (color-magnitude diagram) of the SB9 systems. Based on this distribution, we set the selection criterion in the parameter space in the CMD to engulf the red-giant branch (RGB), asymptotic-giant branch

¹ <https://sb9.astro.ulb.ac.be/>

(AGB), and red clump (RC) and allow for a conservative margin of error in the color index. In total, we identified 1222 systems candidates that potentially are hosting a red giant. We note that such photometric calibration treats the integrated brightness as a single-star source. This simplifying assumption partly explains the larger scatter of the SB9 objects when compared to the well-defined red-giant phases shown from space data in Fig. 1. Furthermore, systems in this regime could also be massive stars, initially OB stars moving horizontally into the super-giant phase. The distribution of the 1222 red-giant candidates in the eccentricity vs orbital-period (e - P) plane is illustrated in Fig. 2.

3. Space photometry

3.1. TESS

The existing full-frame image (FFI) data of the TESS mission up to Sector 40, were searched for all objects on the candidate list, using the `ASTROPY` package (Astropy Collab. et al. 2018). Photometric timeseries for each red-giant candidate were extracted from the FFI data using the `ELEANOR`-package (Feinstein et al. 2019).

`ELEANOR` optimizes the extracted lightcurve for the detection and analysis of exoplanet transit signals. Transit detection requires the highest achievable signal-to-noise ratio possible and, therefore a small aperture around the best-illuminated pixels. García et al. (2014) demonstrated that asteroseismic investigation requires robust lightcurves, achieved by larger apertures. Consequently, we extracted the data forcing a larger aperture than the optimal aperture, determined by `ELEANOR`. TESS FFI data had a cadence of 30 minutes. This was increased to 10 min in the extended mission (years 3-4). To reduce the scatter in the data, we rebinned the 10 min cadence to the classical 30 min cadence.

We selected 77 systems (Table B.1) for which the visual inspection of the power spectrum density (PSD) showed the presence of the acoustic-mode bump below the Nyquist frequency of $283 \mu\text{Hz}$ corresponding to the 30-min cadence for detailed seismic analysis (Sec. 4). To improve the spectral window of the data, gaps of up to two days in the lightcurve were filled through an inpainting technique (García et al. 2014; Pires et al. 2015). Unfortunately, none of the systems in which solar-like oscillations were found, were eclipsing. This might be due to the long orbital periods, compared to the relatively short times-series, provided by TESS.

3.2. Kepler & K2

Similarly, we cross-correlated the candidate list with the NASA *Kepler* data archives, and the re-purposed K2 mission data. This search revealed 16 and 3 known binary systems, respectively with oscillating red-giant primaries (Table B.2). These lightcurves were treated identical to the TESS data. Calibrated lightcurves and their corresponding PSD are available on the MAST archive².

TESS visited the *Kepler* field for 1 or 2 sectors during the second year of its operation. Figure 3 compares two successful detections by both satellites. As expected, the resolution of four years of *Kepler* photometry is superior to a few months of TESS observations. Because the K2 fields are located close to the ecliptic, TESS has not yet observed these targets.

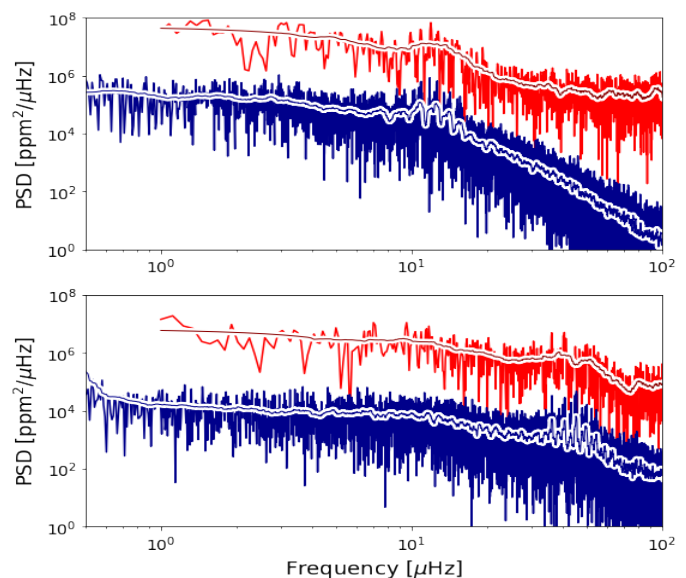


Fig. 3. Power-spectral density for two oscillating red-giant primaries in binary systems. The PSDs of *Kepler* and TESS data are shown in blue and red, respectively. The smoothed power is depicted as a solid line. For better comparison, the TESS-PSD is shifted by two orders of magnitude.

3.3. BRITe

Using BRITe data, Kallinger et al. (2019) could seismically characterize 23 red-giant stars, either through a direct detection of the oscillation-power excess or by measuring the granulation time scales. Among them are two systems which are listed in SB9, 39 Cyg, and 12 Mus.

4. Asteroseismic analysis

While the TESS sample was selected from visual inspection of the PSD, it was not the case for the *Kepler* and K2 targets. Among the *Kepler* and K2 sample, 14 targets and 3 targets respectively exhibit solar-like oscillations. The oscillation signature in the PSD of a solar-like oscillator, as depicted in Fig. 3, is sufficiently characterized through the global seismic parameters (e.g. Aerts et al. 2010, and references therein). The central frequency of the excess oscillation power, ν_{max} is determined from a Gaussian envelope, which is simultaneously fit with two power-laws and a constant offset to describe the granulation signal, the photon noise and the background, respectively (e.g. Carrier et al. 2010). The large-frequency separation, $\Delta\nu$, between modes of the same spherical degree but consecutive radial order (Tassoul 1980) is determined from the power-spectrum of the PSD in the frequency range of the excess of oscillation power (e.g. Mathur et al. 2010). We analysed the `ELEANOR` lightcurves, processed with the standard corrections. For targets with non-significant mode detections, we analyzed the lightcurves, corrected through the principal component analysis (PCA) to remove common instrumental systematics. For all targets, we determined the global seismic parameters using the A2Z pipeline (Mathur et al. 2010).

Using the asteroseismic scaling relations (Kjeldsen & Bedding 1995; Chaplin et al. 2011), the measured ν_{max} and $\Delta\nu$, complemented by the measured effective temperature, T_{eff} allow us to infer the mass and radius for the oscillating star. If available, the effective temperatures were taken from APOGEE (Ahumada et al. 2020). For the remaining targets the effective

² <https://archive.stsci.edu/prepds/kepseismic/>

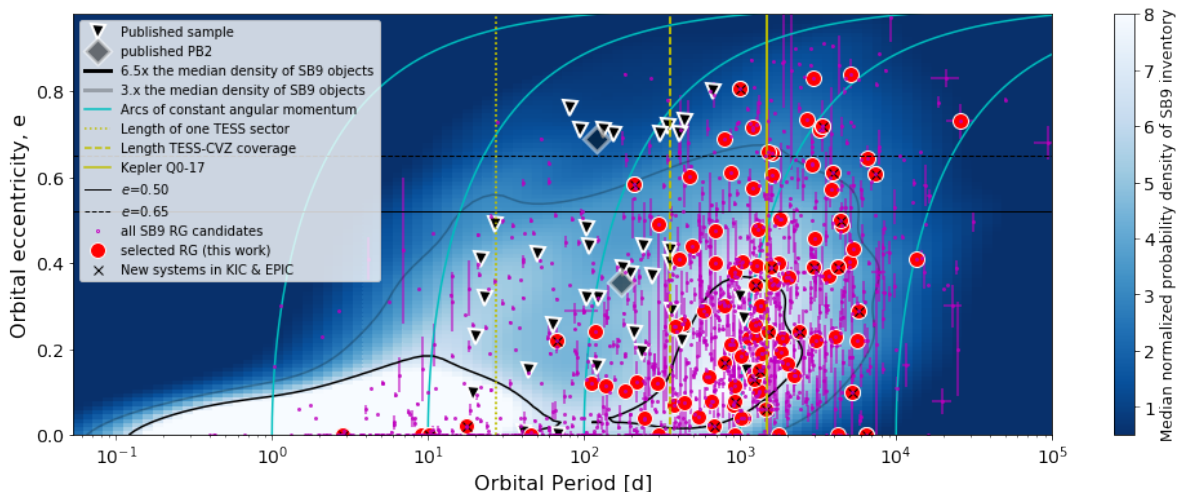


Fig. 4. Distribution of the sample of binary systems, hosting evolved stars as their primary stellar component. Small magenta dots indicate all systems found to host a primary in an advanced stellar evolutionary phase from the photometric calibration described in Sec. 2 and Fig. 1. Red dots mark systems seismically characterized in this study. Systems from the published *Kepler* sample with an oscillating red-giant primary are depicted as black triangles. Systems hosting two oscillating red-giant components (PB2) are shown as gray diamonds. The background density plot represents the distribution of all 4004 systems for which the SB9 (Pourbaix et al. 2004) reports orbital solutions. The gray and black contour lines engulf the regions with 3 and 6.5 times the median density of a bin. The light-blue lines indicate the arcs of constant angular momentum in the e - P plane for circular orbital periods for 1, 10, 100, 1000 and 10000 days. The vertical yellow lines indicate the time span covered by TESS and *Kepler*. The horizontal black lines indicate the range of eccentricities which lack of systems with periods shorter than 200 d.

temperature was taken from the *Gaia* DR2 catalogue, whereby the quoted uncertainty was estimated from the given upper and lower temperature range of the solution. The correction between the asymptotic and observed large-frequency separation was obtained, following Mosser et al. (2013).

The global seismic parameters and the obtained masses and radii for the TESS, *Kepler*, and K2 sample are presented in Table B.1, B.2, respectively. For stars with $\nu_{\max} \leq 10 \mu\text{Hz}$ we only provide an indicative value for ν_{\max} and $\Delta\nu$. Indeed in this frequency regime the detected modes are not in the asymptotic regime (i.e. low n/l). Hence global seismic parameters cannot be directly used in seismic scaling relations. Moreover, short time series as those obtained with a low number of TESS sectors have not enough frequency resolution to properly identify the modes increasing the uncertainties of the inferred seismic quantities.

Table B.3 reports the seismic values from the literature for the targets of BRITE and RV studies. Table B.4 presents additional 15 red-giant candidate systems, which were identified in our photometric search and with existing *Kepler* or K2 data. However, no oscillation were found in these systems.

5. Discussion & Conclusions

The seismic Hertzsprung-Russell diagram (HRD) in Fig. 5 compares the newly established sample of oscillating red-giant stars in binary systems to the 83 systems of the literature sample (see Appendix A). Table A.1 presents 39 previously known systems with determined global seismic parameters and known orbital periods and eccentricities. Table A.2 presents 20 previously known systems for which only the global seismic parameters for the red-giant primary are known. Table A.3 lists 23 previously known systems with very limited parameters known. By adding 99 additional systems to the literature, we have more than doubled the size of the known sample and more than tripled the sample of stars with known global seismic parameters and orbital period and eccentricity.

5.1. Seismic characterization of the sample

The distribution of the systems in Fig. 5 shows that the literature sample, mainly populated the region of $30 \mu\text{Hz} \leq \nu_{\max} \leq 400 \mu\text{Hz}$. The new sample ($\sim 2 \mu\text{Hz} \leq \nu_{\max} \leq 100 \mu\text{Hz}$), presented in this work, extends the sample of oscillating red-giant binaries to lower oscillation frequencies and therefore to the more luminous regime of stars similar to luminous giants like Aldebaran ($\sim 2 \mu\text{Hz}$, Beck et al. 2020). While the analysis of the mixed-mode patterns is beyond the scope of this paper, the position of the new sample in the seismic HRD (Fig. 5) and the wide orbital periods (Fig. 4) suggest that the sample is also rich of He-core burning stars, which have successfully undergone the ignition of the helium core at the tip of the RGB. This lifts the bias on the evolutionary status found in the previous samples. To guide the eye of the reader in the depicted parameter space, Fig. 5 contains evolutionary tracks for 1, 2, and 3 M_{\odot} stars with solar metallicity, which were calculated using MESA (Paxton et al. 2019, and references therein).

It is worth pointing out that eight systems are of the same age, as they are confirmed members of the open cluster NGC 6819. Their membership as well as the cluster's age of ~ 2.3 Gyr have been obtained through asteroseismology by Stello et al. (2011) and Basu et al. (2011), respectively.

5.2. Distribution of the orbital parameters

The distribution of the orbital parameters of the systems in the e - P plane is depicted in Fig. 4. The background contour plot illustrates the distribution of all orbits listed in the SB9 catalog. The majority of systems have periods below ~ 100 days with low-eccentricities or even circularized orbits ($e \leq 0.2$). This over-density is mostly populated with hot stars below the spectral type F, whose structure is dominated by radiative regions (Torres et al. 2010).

All candidate red-giant systems, which were identified from the CMD in Sec. 2 are shown as small magenta dots in Fig. 4.

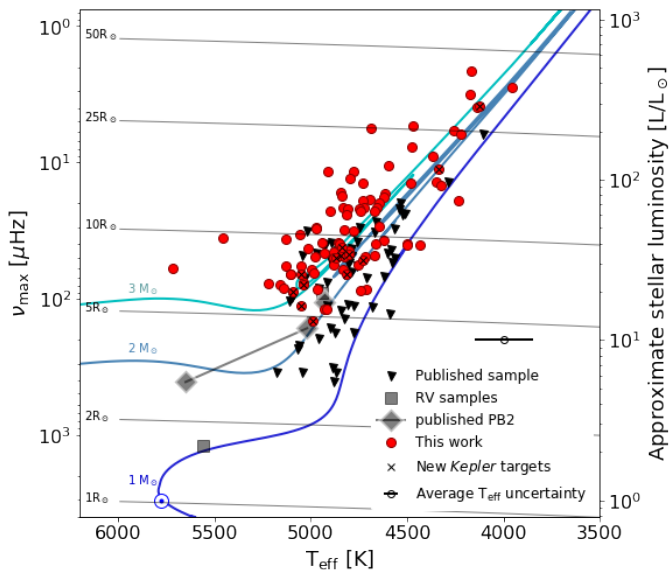


Fig. 5. Distribution of the sample in the seismic HRD with the frequency of the oscillation-power excess on the left vertical axis. The symbols are identical to Fig. 4. The bottom marker indicates the average uncertainty of the effective temperature of 150K. For reference, lines of constant radius and evolutionary tracks for solar metallicity are shown for 1, 2, and 3 M_{\odot} stars. The approximately equivalent stellar luminosity is indicated on the right vertical axis.

Uncertainties are not available for the first systems listed in the SB9 catalog, but are provided for more recent entries. While a few red-giant systems share the same region in the parameter space as the bulk of the hot binaries, most of the evolved stars are found in systems with orbital periods $200 \text{ d} \leq P_{\text{orb}} \leq 3000 \text{ d}$, and $e \leq 0.6$. This rich sample of evolved stars form a second, teardrop-shaped overdensity found in the distribution of the SB9 systems. In addition, in this period regime, the SB9 catalogue contains systems that cover the entire possible range, from circularized orbits ($e=0$) to a reported maximum of $e_{\text{max}} = 0.972$.

Figure 4 illustrates the differences in the orbital parameters of the sample, collected from previous literature and systems analyzed in this work. Both samples show a similar distribution in the covered range of eccentricities. Stars in the *Kepler* sample have been selected due to their photometric binary signatures, such as periodically occurring eclipses or heartbeat events. Such selection constraints prefer systems with periods shorter than the time base of the mission (shown as yellow vertical lines in Fig. 4). Because a red-giant will expand its radius by two orders of magnitude, as it advances on the RGB, it is unlikely that systems with such periods will survive the unavoidable common-envelope phase unaltered. Therefore, it is not surprising that the *Kepler* sample predominantly contains stars in the rapidly evolving H-shell burning RGB phase (Beck et al. 2018b) and contains a lower number of stars, quiescently burning He in the core and maintaining a stable luminosity. From the full catalogue of published systems in App. A, we find that 38 RGB and 13 RC systems were identified.

Selecting systems based on the a-priori knowledge of their spectroscopically-inferred binary nature removes the bias on the period, previously introduced by the observation length of space photometry from our sample of binary systems, characterized through asteroseismology. This selection also removes the bias that they are eclipsing, which also depends on the inclination angle. Therefore, systems with very long periods can be studied

by asteroseismology with the single requirement that the photometric time series allows for a frequency resolution, sufficient to perform asteroseismic analysis. Only for very close systems, typically $P \leq 20 \text{ days}$, the magnetic activity, which is increased because of the acceleration of rotation triggered by tides that strengthens the dynamo action through a tidally driven dynamo, will suppress solar-like oscillations (Gaulme et al. 2016; Mathur et al. 2019; Benbakoura et al. 2021). Extending the sample with systems with periods of several hundred to thousands of days opens the analysis to wider binary systems whose primary likely has already progressed through the RGB and is now quiescently burning helium in its core.

6. A red-giant desert in the e - P plane?

It was pointed out by Beck et al. (2018b) and Benbakoura et al. (2021) that the *Kepler* sample of red-giant binaries does not contain systems with $0.5 \leq e \leq 0.7$ (for $P_{\text{orb}} \leq 200 \text{ d}$). This apparent gap, which we will refer to as *red-giant desert*, poses an interesting puzzle.

The small number of red-giant binaries in the *Kepler* sample (black triangles in Fig. 4) hindered further conclusions. The *Kepler* sample (black triangles) only extended to orbital periods of about 400 d, which made the feature appear more pronounced but had the problem of small number statistics. This study increased the number of stars identified in advanced evolutionary stages by two orders of magnitude, which extends to much larger eccentricities. However, the region $P_{\text{orb}} \leq 200 \text{ d}$, $e \geq 0.5$ remains sparsely populated.

Tidal circularization reflects the interplay of two bodies and the dissipation of the kinetic energy of tidal flows into heat. Unless a third body is acting on the system or mass is lost, tidal forces should reduce eccentricity. Tidal theory, therefore, does not predict such a gap. Spiraling of the secondary onto the primary of the system would occur when the total angular momentum of the orbital movement is less than three times the total angular momentum from the stellar rotation (Hut 1980), which is not the case for these systems.

The long-periodic edge of the gap at $\sim 200 \text{ d}$ is explainable as the time scales of the tidally-driven circularization are becoming too long lived to show immediate effects (Beck et al. 2018b). This region in the e - P diagram ($P_{\text{orb}} \leq 200 \text{ d}$, $e \geq 0.5$) is also less populated by stars on the main-sequence, as can be seen from the iso-contour of the total distribution. The bottom edge at $e \approx 0.5$ coincides with the sudden drop in the population in the e - P plane.

Can detection bias affect the distribution? One possible bias is the detectability of a binary system from spectroscopy. With an increasing eccentricity and longer orbital period, the duration in which the binary system shows negligible variations of its radial velocities are growing. Unless measured to a high RV precision, such systems could go unnoticed from a short-term sampling survey. This is, in particular the case, if we are facing the long side of the ellipse. Yet, such an argument would instead explain a lower occurrence rate at longer periods. The red-giant desert, however is found at periods compatible with the typical length of an observing season. Also, even a relatively sparse sampling could reveal a binary system.

Contrary to what might be expected from the large number of red-giant systems in the SB9, there are about as many systems found from *Kepler* as listed in the SB9. This might still point to a selection bias as those systems were selected due to their heartbeat signature in the light curve. Human bias might

Table 1. Periastron distance and radius of the Roche lobe between both components of a hypothetical system.

| e [] | $P_{\text{orbit}}=150$ d | | $P_{\text{orbit}}=500$ d | | $P_{\text{orbit}}=1000$ d | |
|------------|-----------------------------------|---|-----------------------------------|---|-----------------------------------|---|
| | S_{peri} [R_{\odot}] | $R_{L,1}^{\text{Peri}}$ [R_{\odot}] | S_{peri} [R_{\odot}] | $R_{L,1}^{\text{Peri}}$ [R_{\odot}] | S_{peri} [R_{\odot}] | $R_{L,1}^{\text{Peri}}$ [R_{\odot}] |
| 0.2 | 123.6 | 50.8 | 275.8 | 113.4 | 437.9 | 180.0 |
| 0.4 | 92.7 | 38.1 | 206.9 | 85.0 | 328.4 | 135.0 |
| 0.6 | 61.8 | 25.4 | 137.9 | 56.7 | 218.9 | 90.0 |
| 0.8 | 30.9 | 12.7 | 68.9 | 28.3 | 109.3 | 44.9 |

Notes. A hypothetical binary system of $M_1=1.3M_{\odot}$ and $M_2=0.9M_{\odot}$ is assumed to calculate the separation between both components S_{peri} and the corresponding radius of the Roche lobe for the primary ($R_{L,1}^{\text{Peri}}$) component are calculated for a grid in period (P_{orb} : 150, 500, and 1000 d) and orbital eccentricity (e : 0.2, 0.4, 0.6, and 0.8) during periastron. All values are given in solar units.

explain this. Systems in the red-giant desert are typically heart-beat stars. While one has to make the effort of selecting them for RV monitoring, their photometric signature simply is a byproduct of light-curve analysis of space data.

Table 1 describes the separation and the radius of the Roche lobe (in the formulation of Eggleton 1983) around the giant primary between two components of a hypothetical binary system, consisting of a primary and secondary of 1.3 and $0.9M_{\odot}$ on a 150, 500 and 1000 day orbit with four different eccentricities of 0.2, 0.4, 0.6, and 0.8. Provided that a star at the tip of the RGB reaches a maximum radius of $\sim 170R_{\odot}$, it can be seen that at some point, the giant will fill its Roche lobe. The mass transfer onto the secondary during this phase of stable Roche lobe overflow (Han et al. 2002), will drive a rapid decrease of the orbital eccentricity. Suppose the modified system with lower eccentricity is still too small for the maximum radius of the giant primary. In that case, the system will undergo a common-envelope phase, which most likely leads to the ejection of the system and the creation of a hot subdwarf B star (Han et al. 2002).

We note that all published systems from the *Kepler* sample found above (i.e. $e \geq 0.4$, $P_{\text{orb}} \leq 200$ d) the red-giant desert were indeed identified as H-shell burning stars (Beck et al. 2018b). This supports the idea that the region was deserted of red-giant stars due to the expanding stellar radius.

7. Outlook

With this work, we have substantially increased the number of known red-giant stars in binary systems, characterized through space photometry.

Due to the way we selected the sample only based on SB9 and CMD, most of our systems do not present eclipses in the light curves. The unconstrained inclination of the orbit along the line of sight, therefore, poses limitations for further exploiting the full potential of the ensemble. Because the scaling relations treat the oscillating component as a single source, the astroseismic investigation of the red-giant components delivers inclination-independent masses and radii. Specifically, through constraints set by binarity on the initial conditions and through accurate orbital solutions detailed modelling of the complex internal physics will be possible (White et al. 2013; Beck et al. 2018a).

For studies of tidal forces, which scale with the sixth power of the radius (Zahn 2013), such large ensembles of systems with seismically inferred radii and a clear identification of the evolutionary state in a wide range of eccentricities will provide important test cases. As tidal interactions strengthen the dynamo, we also expect to find many spotted stars, which will allow us to study synchronization and angular momentum transport in stars.

When the astrometric timeseries from *Gaia* DR3 (expected for 2022) arrive, we predict that we will be able to infer the inclination from the shape of the projected binary orbit and the known orbital eccentricity from spectroscopic solutions for wider binaries. This growing catalogue of seismically characterized systems is, therefore, an important step in preparing ensemble asteroseismology red-giant binaries for the advent of *Gaia* DR3. The approach, presented in this paper also allows a targeted search for oscillators in binary systems with the forthcoming ESA PLATO mission (Rauer et al. 2014). The multicolor photometry of this mission will be of high value to the study of oscillations and binary modelling.

Extending the sample coverage towards longer periods and enriching the sample with He-core burning stars will, therefore, open a treasure trove to study open questions of stellar structure and its evolution.

Acknowledgements. We thank the referee for useful comments that allowed us to improve the article. PGB supports the financial support by NAWI Graz and acknowledges the support by the *Dr. Heinrich-Jörg Foundation* at the faculty of natural sciences at Graz University. SM acknowledges support by the Spanish Ministry of Science and Innovation with the *Ramón y Cajal* fellowship number RYC-2015-17697 and the grant number PID2019-107187GB-I00. RAG and StM acknowledge support from the PLATO CNES grant. This paper includes data collected with the *Kepler* & TESS missions, obtained from the MAST data archive at the Space Telescope Science Institute (STScI). KH acknowledges support through NASA ADAP grants (80NSSC19K0594). Funding for these missions is provided by the NASA Science Mission Directorate and by the NASA Explorer Program respectively. STScI is operated by the Association of Universities for Research in Astronomy, Inc., under NASA contract NAS 5-26555. Based on data collected by the BRITE Constellation satellite mission, designed, built, launched, operated and supported by the Austrian Research Promotion Agency (FFG), the University of Vienna, the Technical University of Graz, the University of Innsbruck, the Canadian Space Agency (CSA), the University of Toronto Institute for Aerospace Studies (UTIAS), the Foundation for Polish Science & Technology (FNiTP MNiSW), and National Science Centre (NCN).

Software: Python (Van Rossum & Drake 2009), numpy (Oliphant 2006; Harris et al. 2020), matplotlib (Hunter 2007), scipy (Virtanen et al. 2020), astropy (Astropy Collaboration et al. 2013, 2018). This research made use of Astropy, a community-developed core Python package for Astronomy.

References

- Aerts, C., Christensen-Dalsgaard, J., & Kurtz, D. W. 2010, *Asteroseismology*
 Ahumada, R., Prieto, C. A., Almeida, A., et al. 2020, *ApJS*, 249, 3
 Astropy Collab., Price-Whelan, A. M., Sipőcz, B. M., et al. 2018, *AJ*, 156, 123
 Astropy Collaboration, Price-Whelan, A. M., Sipőcz, B. M., et al. 2018, *aj*, 156, 123
 Astropy Collaboration, Robitaille, T. P., Tollerud, E. J., et al. 2013, *A&A*, 558, A33
 Badenes, C., Mazzola, C., Thompson, T. A., et al. 2018, *ApJ*, 854, 147
 Basu, S., Grundahl, F., Stello, D., et al. 2011, *ApJ*, 729, L10
 Beck, P. G., Hambleton, K., Vos, J., et al. 2014, *A&A*, 564, A36
 Beck, P. G., Hambleton, K., Vos, J., et al. 2015a, 101, 06004
 Beck, P. G., Kallinger, T., Pavlovski, K., et al. 2018a, *A&A*, 612, A22
 Beck, P. G., Kambe, E., Hillen, M., et al. 2015b, *A&A*, 573, A138

- Beck, P. G., Kuschnig, R., Houdek, G., et al. 2020, in *Stars and their Variability Observed from Space*, ed. C. Neiner, W. W. Weiss, D. Baade, R. E. Griffin, C. C. Lovekin, & A. F. J. Moffat, 75–79
- Beck, P. G., Mathis, S., Gallet, F., et al. 2018b, *MNRAS*, 479, L123
- Benbakoura, M., Gaulme, P., McKeever, J., et al. 2021, *A&A*, 648, A113
- Borucki, W. J., Koch, D., Basri, G., et al. 2010, *Science*, 327, 977
- Brogaard, K., Hansen, C. J., Miglio, A., et al. 2018, *MNRAS*, 476, 3729
- Carrier, F., De Ridder, J., Baudin, F., et al. 2010, *A&A*, 509, A73
- Chaplin, W. J., Kjeldsen, H., Christensen-Dalsgaard, J., et al. 2011, *Science*, 332, 213
- Christensen-Dalsgaard, J. 1984, in *Space Research in Stellar Activity and Variability*, ed. A. Mangeney & F. Praderie, 11
- Eggleton, P. P. 1983, *ApJ*, 268, 368
- Feinstein, A. D., Montet, B. T., Foreman-Mackey, D., et al. 2019, *PASP*, 131, 094502
- Frandsen, S., Lehmann, H., Hekker, S., et al. 2013, *A&A*, 556, A138
- Gaia Collaboration, Brown, A. G. A., Vallenari, A., et al. 2018, *A&A*, 616, A1
- García, R. A., Mathur, S., Pires, S., et al. 2014, *A&A*, 568, A10
- Gaulme, P. & Guzik, J. A. 2019, *A&A*, 630, A106
- Gaulme, P., Jackiewicz, J., Appourchaux, T., & Mosser, B. 2014, *ApJ*, 785, 5
- Gaulme, P., Jackiewicz, J., Spada, F., et al. 2020, *A&A*, 639, A63
- Gaulme, P., McKeever, J., Jackiewicz, J., et al. 2016, *ApJ*, 832, 121
- Gaulme, P., McKeever, J., Rawls, M. L., et al. 2013, *ApJ*, 767, 82
- Han, Z., Podsiadlowski, P., Maxted, P. F. L., Marsh, T. R., & Ivanova, N. 2002, *MNRAS*, 336, 449
- Harris, C. R., Millman, K. J., van der Walt, S. J., et al. 2020, *Nature*, 585, 357–362
- Howell, S. B., Sobek, C., Haas, M., et al. 2014, *PASP*, 126, 398
- Hunter, J. D. 2007, *Computing in Science Engineering*, 9, 90
- Hut, P. 1980, *A&A*, 92, 167
- Johnston, C., Pavlovski, K., & Tkachenko, A. 2019, *A&A*, 628, A25
- Kallinger, T., Beck, P. G., Hekker, S., et al. 2019, *A&A*, 624, A35
- Kallinger, T., Beck, P. G., Stello, D., & García, R. A. 2018, *A&A*, 616, A104
- Kirk, B., Conroy, K., Prša, A., et al. 2016, *AJ*, 151, 68
- Kjeldsen, H. & Bedding, T. R. 1995, *A&A*, 293, 87
- Kumar, P., Ao, C. O., & Quataert, E. J. 1995, *ApJ*, 449, 294
- Mackereth, J. T., Miglio, A., Elsworth, Y., et al. 2021, *MNRAS*, 502, 1947
- Mathur, S., García, R. A., Bugnet, L., et al. 2019, *FrASS*, 6, 46
- Mathur, S., García, R. A., Régulo, C., et al. 2010, *A&A*, 511, A46
- Mosser, B., Michel, E., Belkacem, K., et al. 2013, *A&A*, 550, A126
- Oliphant, T. 2006, *NumPy: A guide to NumPy, USA: Trelgol Publishing*
- Paxton, B., Smolec, R., Schwab, J., et al. 2019, *ApJS*, 243, 10
- Pires, S., Mathur, S., García, R. A., et al. 2015, *A&A*, 574, A18
- Pourbaix, D., Tokovinin, A. A., Batten, A. H., et al. 2004, *A&A*, 424, 727
- Prša, A., Batalha, N., Slawson, R. W., et al. 2011, *AJ*, 141, 83
- Prša, A. 2018, *PHOEBE 2 - Modeling and Analysis of Eclipsing Binary Stars*
- Rauer, H., Catala, C., Aerts, C., et al. 2014, *Experimental Astronomy*, 38, 249
- Rawls, M. L., Gaulme, P., McKeever, J., et al. 2016, *ApJ*, 818, 108
- Ricker, G. R., Winn, J. N., Vanderspek, R., et al. 2014, in *SPIE 914320*
- Silva Aguirre, V., Stello, D., Stokholm, A., et al. 2020, *ApJ*, 889, L34
- Stello, D., Meibom, S., Gilliland, R. L., et al. 2011, *ApJ*, 739, 13
- Tassoul, M. 1980, *ApJS*, 43, 469
- Thermon, N., Hekker, S., Southworth, J., et al. 2018, *MNRAS*
- Thompson, S. E., Everett, M., Mullally, F., et al. 2012, *ApJ*, 753, 86
- Torres, G., Andersen, J., & Giménez, A. 2010, *A&Ar*, 18, 67
- van Leeuwen, F. 2007, *A&A*, 474, 653
- Van Rossum, G. & Drake, F. L. 2009, *Python 3 Reference Manual* (Scotts Valley, CA: CreateSpace)
- Virtanen, P., Gommers, R., Oliphant, T. E., et al. 2020, *Nature Methods*, 17, 261
- Weiss, W. W., Rucinski, S. M., Moffat, A. F. J., et al. 2014, *PASP*, 126, 573
- White, T. R., Huber, D., Maestro, V., et al. 2013, *MNRAS*, 433, 1262
- Yu, J., Huber, D., Bedding, T. R., et al. 2018, *ApJS*, 236, 42
- Zahn, J.-P. 2013, in *Lecture Notes in Physics*, Vol. 861, 301

Appendix A: Catalogue of oscillating red-giant binaries in the literature

In the scientific literature, currently 83 systems with an oscillating red-giant star are known. The Tables A.1, A.2, and A.3, cite in which papers a system has been seismically analysed, using the following abbreviations. The references for the quoted values stands as first, other references for this star follow in the bracket. Beck et al. (2014, B14), Beck et al. (2015b, B15a), Beck et al. (2015a, B15b), Beck et al. (2018a, B18), Frandsen et al. (2013, F13), Gaulme et al. (2013, G13), Gaulme et al. (2014, G14), Gaulme et al. (2016, G16), Rawls et al. (2016, R16), Gaulme & Guzik (2019, GG19), Gaulme et al. (2020, G20), Benbakoura et al. (2021, B21), Brogaard et al. (2018, Br18), and Themeßl et al. (2018, T18).

In addition the already described parameters, Tables A.1 and A.2 also report the evolutionary status, discriminating between RGB and RC red-giant primaries, the value of the asymptotic period spacing of gravity dipole modes, $\Delta\Pi_1$ and the mass ratio for each system, M_2/M_1 .

Appendix B: Catalogue of new oscillating red-giant binaries

Tables B.1, B.2, B.3, and B.4 share the following elements. Additional content is explained in the table notes of each table. The first vertical panel of the tables provides various stellar identifiers.

- The star’s sequence number in the SB9 catalogue and the identifier in the *TESS Input Catalogue* (TIC) are provided in the first two columns.
- Additionally, in Table B.2, and B.4, the TIC identifier is followed by the star’s identifier in the *Kepler Input Catalogue* (KIC), *Ecliptic Input Catalogue* (EPIC), respectively. Table B.3 provides an alternative identifier for the bright stars in the Bayer or Flamsteed catalogue.

The next vertical panel provides information on the observations. Further literature values are provided for a better characterization of the objects.

- The next column provides information on the length of the data set. Table B.1 lists the number of *TESS Sectors* with the typical length of 27.5 d each, or Table B.2 provides the number of the so called *Kepler Quarters* with the typical length of 90 d, each. As Table B.3 summarizes various results, we refer the reader to the notes below the table for more details.
- The apparent magnitude in Johnson V, as reported in the Simbad Catalog, is given.
- The column T_{eff} gives the effective temperature of the star in Kelvin.

The third vertical panel reports the observed and derived seismic quantities and the period of long periodic variations

- The column labeled as ‘ ν_{max} ’ and ‘ $\Delta\nu$ ’ report the peak frequency of the oscillation-power excess and large-frequency separation with their respective uncertainties. Because the giant is by far the brighter component, we can safely assume that the oscillations originate from the primary. In case no oscillation pattern could be detected, the field is filled with a ‘–’. The seismic extraction pipeline A2Z is underestimating the uncertainties for luminous red-giants. In a conservative approach, we decided only to report the value but not provide an uncertainty for them.

- The columns M , R , and $\log g$ report the seismically inferred values for the mass, radius and surface gravity of the primary star in solar units. ($\nu_{\text{max},\odot}=3100\mu\text{Hz}$, $\Delta\nu_{\odot}=135.2\mu\text{Hz}$ and 5777 K for the effective temperature of the Sun).

The last five columns report the orbital parameters as given in the SB9 catalogue.

- P_{orb} and e describe the period and eccentricity of the orbit, respectively.
- K_1 reports the radial velocity amplitude of the primary stellar component. K_2 reports the RV amplitude of the secondary, if known. No uncertainties are provided in the SB9 for K_1 and K_2 .
- The last column reports the Grade of the solution, reported by SB9. It ranges between poor (grade = 0) and definitive (5). If no value was available, the field is filled by –.

Table A.1. Red-giant binary systems with determined seismic and orbital parameters.

| KIC | Typ | Evol. State | V [mag] | T_{eff} [K] | ν_{max} [μHz] | $\Delta\nu$ [μHz] | $\Delta\Pi_1$ [s] | P_{orb} [d] | e | M_2/M_1 | Literature References |
|----------|--------------|-------------|---------|----------------------|---------------------------------------|--------------------------------|-------------------|-------------------------|---------------------|------------------|-------------------------------------|
| 9163796A | HB, SB2, PB2 | RGB | 9.8 | 5020 ± 100 | 165.3 ± 1.3 | 12.85 ± 0.03 | | 121.30 ± 0.01 | 0.692 ± 0.002 | 0.99 ± 0.005 | B18 (B14, GG19) |
| 9163796B | | RGB | | 5650 ± 70 | 410 ± 50 | | | | | | |
| 9246715A | EC, SB2, PB2 | RC | 9.7 | 4930 ± 230 | 106.4 ± 0.8 | 8.3 ± 0.02 | | 171.27688 ± 0.00001 | 0.3559 ± 0.0003 | 0.90 ± 0.001 | R16 (G13, G14, GG19) |
| 9246715B | | RC | | 4930 ± 230 | 106.4 ± 0.8 | | | | | | |
| 2444348 | HB | RGB | 10.7 | 4565 | 30.5 ± 0.3 | 3.26 ± 0.01 | | 103.50 ± 0.01 | 0.48 ± 0.01 | | B14 (GG19) |
| 2697935 | EC, HB | RGB | 11.0 | 4883 | 405.6 ± 3 | 28 | | 21.50 ± 0.01 | 0.41 ± 0.02 | | B14 (GG19) |
| 2720096 | HB | RGB | 4812 | | 110.1 ± 0.7 | 9.17 ± 0.01 | | 26.70 ± 0.01 | 0.49 ± 0.01 | | B14 (GG19) |
| 4054905 | SB2, EC | RC | 4790 | ± 190 | 48.13 ± 0.21 | 5.42 ± 0.01 | 159.5 | 274.7306 ± 0.0004 | 0.372 ± 0.002 | 0.98 | B21 (GG19) |
| 4360072 | EC | RC | 5020 | ± 210 | 31.81 ± 0.06 | 3.90 ± 0.01 | 392.2 | 1084.76 ± 0.01 | 0.152 ± 0.001 | | B21 (GG19) |
| 4663623 | EC, SB2 | RGB | 11.5 | 4803 | ± 91 | 54.09 ± 0.24 | 5.212 ± 0.019 | 358.09 ± 0.0003 | 0.43 ± 0.01 | 0.99 ± 0.08 | G16 (G13) |
| 4663623 | SB2, EC | RC | 4812 | ± 92 | 54.09 ± 0.24 | 5.21 ± 0.02 | 363.6 | 358.0900 ± 0.0001 | 0.399 ± 0.001 | $0.96 \pm$ | B21 (G14, G16, B18, GG19) |
| 5006817 | HB | RGB | 11.2 | 5000 | 145.9 ± 0.5 | 11.64 ± 0.01 | | 94.812 ± 0.002 | 0.7069 ± 0.0002 | | B14 (GG19) |
| 5039392 | HB | RGB | 4110 | | 6.2 ± 0.1 | 1.13 ± 0.01 | | 236.70 ± 0.02 | 0.44 ± 0.01 | | B14 (GG19) |
| 5179609 | EC, SB2 | RGB | 4887 | ± 91 | 321.84 ± 1 | 22.21 ± 0.05 | | 43.931080 ± 0.00002 | 0.15 ± 0.001 | 0.51 ± 0.02 | G16 (G13, G14, B21, GG19) |
| 5308778 | EC, SB2 | RGB | 5044 | ± 91 | 48.47 ± 1.1 | 5.05 ± 0.05 | | 40.5661 ± 0.0003 | 0.006 ± 0.005 | 0.43 ± 0.03 | G16 (G13, G14, B21, GG19) |
| 5640750 | EC | RGB | 11.9 | 4525 | ± 75 | 24.1 ± 0.2 | 2.969 | 987.398 ± 0.006 | 0.322 ± 0.008 | 0.85 ± 0.03 | T18 (G13, G14, G16, B21, T18, GG19) |
| 5786154 | EC, SB2 | RGB | 4747 | ± 100 | 29.75 ± 0.16 | 3.52 ± 0.01 | | 197.9180 ± 0.0004 | 0.3764 ± 0.0009 | 0.96 ± 0.07 | G16 (G13, G14, B21, GG19) |
| 5866138 | EC | RC | 11.5 | 4960 | ± 120 | 83.71 ± 0.46 | 272.4 | 342.259 ± 0.008 | 0.7158 ± 0.0004 | | B21 (GG19) |
| 6757558 | EC | RGB | 4590 | ± 110 | 129.38 ± 0.28 | 11.28 ± 0.01 | 80.1 | 421.190 ± 0.009 | 0.22 ± 0.03 | | B21 (GG19) |
| 7037405 | EC, SB2 | RGB | 4516 | ± 36 | 21.75 ± 0.14 | 2.79 ± 0.01 | | 207.1083 ± 0.0007 | 0.238 ± 0.004 | 0.91 ± 0.04 | G16 (G13, G14, B21, GG19) |
| 7293054 | SB2, EC | ? | 11.6 | 4790 | ± 160 | 42.58 ± 0.27 | | 671.806 ± 0.003 | 0.8 ± 0.01 | $0.84 \pm$ | B21 (GG19) |
| 7377422 | EC, SB2 | RGB | 4938 | ± 110 | 40.1 ± 2.1 | 4.64 ± 0.05 | | 107.6213 ± 0.0004 | 0.4377 ± 0.0005 | 0.81 ± 0.07 | G16 (G14, GG19) |
| 7768447 | EC | ? | 12.0 | 4760 | ± 160 | 57.79 ± 0.52 | | 122.32 ± 0.04 | 0.322 ± 0.009 | | B21 (GG19) |
| 8054233 | EC, SB2 | RGB | 4971 | ± 90 | 46.49 ± 0.33 | 4.81 ± 0.015 | | 1058.16 ± 0.02 | 0.2718 ± 0.004 | 0.69 ± 0.04 | G16 (G14, GG19) |
| 8095275 | HB | RGB | 4622 | | 69.3 ± 0.3 | 6.81 ± 0.01 | | 23.00 ± 0.01 | 0.32 ± 0.01 | | B14 (G13, B14, GG19) |
| 8144355 | HB | RGB | 4875 | | 179 ± 2 | 13.95 ± 0.04 | | 80.55 ± 0.01 | 0.76 ± 0.01 | | B14 (GG19) |
| 8210370 | HB | RGB | 11.4 | 4585 | 44.1 ± 0.8 | 4.69 ± 0.02 | | 153.50 ± 0.01 | 0.7 ± 0.01 | | B14 (GG19) |
| 8410637 | EC | RGB | 11.3 | 4605 | ± 80 | 46.4 ± 0.3 | 4.564 | 408.3248 ± 0.0004 | 0.686 ± 0.001 | 0.89 ± 0.01 | T18 (F13, G13, G14, B21, GG19) |
| 8430105 | EC, SB2 | RGB | 10.6 | 5042 | ± 68 | 76.7 ± 0.57 | 7.14 | 63.32713 ± 0.0003 | 0.2564 ± 0.0002 | 0.63 ± 0.01 | G16 (G13, G14, B21, GG19) |
| 8702921 | EC, SB2 | RGB | 5058 | ± 86 | 195.57 ± 0.47 | 14.07 ± 0.01 | | 19.38446 ± 0.00002 | 0.0964 ± 0.0008 | 0.16 ± 0.01 | G16 (G13, G14, B21, GG19) |
| 8912308 | HB | RGB | 11.8 | 4872 | 350 ± 9 | 22.7 | | 20.17 ± 0.01 | 0.23 ± 0.01 | | B14 (GG19) |
| 9151763 | HB | RGB? | 4290 | | 13.8 ± 0.2 | 1.98 ± 0.01 | | 437.51 ± 0.03 | 0.73 ± 0.01 | | B14 (GG19) |
| 9153621 | SB2, EC | ? | 4760 | ± 190 | 38.22 ± 0.3 | 4.28 ± 0.01 | | 305.792 ± 0.005 | 0.7 ± 0.003 | 0.86 | B21 (GG22) |
| 9408183 | HB | RGB | 4900 | | 164.8 ± 0.2 | 13.29 ± 0.02 | | 49.70 ± 0.01 | 0.42 ± 0.01 | | B14 (GG19) |
| 9540226 | EC, SB2 | RGB | 12.4 | 4692 | ± 65 | 27.07 ± 0.15 | 3.22 | 175.4439 ± 0.0006 | 0.388 ± 0.0002 | 0.74 ± 0.04 | G16 (G13, G14, B14, T18, GG19) |
| 9904059 | EC | RGB | 4830 | ± 160 | 140.61 ± 0.45 | 11.91 ± 0.01 | 79.8 | 102.963 ± 0.001 | 0.32 ± 0.01 | | B21 (GG19) |
| 9970396 | EC, SB2 | RGB | 4916 | ± 68 | 63.70 ± 0.16 | 6.32 ± 0.01 | | 235.2985 ± 0.0002 | 0.194 ± 0.007 | 0.89 ± 0.03 | G16 (G13, G14, B21, GG19) |
| 10001167 | EC, SB2 | RGB | 10.4 | 4700 | ± 66 | 19.90 ± 0.09 | 2.762 | 120.3903 ± 0.0005 | 0.159 ± 0.003 | 0.98 ± 0.07 | G16 (G13, G14, GG19) |
| 10015516 | EC | RC | 10.9 | 4830 | ± 130 | 66.85 ± 0.67 | 294.5 | 67.69217 ± 0.00009 | 0 ± 0.01 | | B21 (GG19) |
| 10074700 | EC | ? | 5070 | ± 100 | 232 ± 2 | 18.37 ± 0.02 | | 365.6340 ± 0.0006 | 0.29 ± 0.06 | | B21 (GG19) |
| 10614012 | EC, HB | RGB | 10.0 | 4715 | 70.2 ± 0.9 | 6.54 ± 0.02 | | 132.13 ± 0.01 | 0.71 ± 0.01 | | B14 (GG19) |

Beck et al.: Oscillating red-giant stars in binary systems with NASA TESS and NASA Kepler

Table A.2. Catalogue and parameters for oscillating red-giant binaries characterized through photometry from the *Kepler* mission.

| KIC | Typ | Evol. State | V [mag] | T _{eff} [K] | ν_{\max} [μ Hz] | $\Delta\nu$ [μ Hz] | $\Delta\Pi_1$ [s] | P _{orb} [d] | <i>e</i> | M ₂ /M ₁ | Literature References |
|----------|-----|-------------|---------|----------------------|--------------------------|-------------------------|-------------------|----------------------|----------|--------------------------------|-----------------------|
| 7431665 | HB | RGB | 11.3 | 4580 | 54.0 ± 0.7 | 5.46 ± 0.02 | | 281.4 | | | B14 (GG19) |
| 7799540 | HB | RGB | | 5177 | 347.2 ± 5 | 24 | | 71.8 | | | B14 (GG19) |
| 8803882 | HB | RGB | | 5043 | 347.0 ± 3 | 22.6 ± 0.4 | | 89.7 | | | B14 (GG19) |
| 11044668 | HB | RGB? | 11.9 | 4565 | 50.2 ± 0.2 | 5.56 ± 0.01 | | 139.5 | | | B14 (GG19) |
| 8108336 | | ? | | 4868 ± 170 | 46.6 ± 0.57 | 4.5 | | | | | G20 |
| 8515227 | | RGB | 11.5 | 4778 | 176 ± 2 | 14.6 | 82.2 | | | | G20 |
| 9837673 | | RGB | | 5062 | 222 ± 2 | 15.13 | 96.1 | | | | G20 |
| 10198347 | | RC | 10.6 | 4924 | 39.65 ± 0.5 | 4.47 | 276.6 | | | | G20 |
| 10811720 | | ? | 12.2 | 4893 | 38.98 ± 0.33 | 4.37 | | | | | G20 |
| 12314910 | | ? | 11.6 | 4514 | 23.96 ± 0.25 | 2.97 | | | | | G20 |
| 3458643 | | RC | 10.5 | 5035 | 70 ± 2 | 5.82 | 213.9 | | | | G20 |
| 3967501 | | RC | | 4682 | 115 ± 8 | 9.95 | 146.9 | | | | G20 |
| 4242873 | | RGB | | 4848 | 121.48 ± 0.89 | 10.56 | 63.9 | | | | G20 |
| 5382824 | | RC | 10.7 | 5114 | 104.05 ± 0.81 | 7.9 | 252.2 | | | | G20 |
| 5439339 | | RC | 11.3 | 5098 | 99 ± 1 | 7.86 | 250.2 | | | | G20 |
| 6032639 | | RC | 11.4 | 4862 | 45 ± 0.68 | 4.77 | 289.8 | | | | G20 |
| 6590195 | | RGB | 12.5 | 4779 | 113.11 ± 0.6 | 9.54 | | | | | G20 |
| 6933666 | | ? | | 4668 | 32.6 ± 0.39 | 3.87 | | | | | G20 |
| 7103951 | | RC | 9.6 | 4902 | 52.7 ± 0.57 | 5.11 | 304.1 | | | | G20 |
| 7948193 | | RGB? | 11.1 | 4921 | 113.7 ± 0.87 | 9.09 | | | | | G20 |

Table A.3. Catalogue of red-giant binary system with limited information in the literature.

| KIC | Type | T _{eff} [K] | P _{orbit} [days] | Reference Comments |
|----------|------|----------------------|---------------------------|-----------------------------|
| 3851949 | EC | 4981 | 54.77 | GG19 |
| 4078157 | EC | 5547 | 16.02 | GG19 |
| 4769799 | EC | 4911 | 21.93 | GG19 |
| 4999260 | EC | 5048 | 0.38 | GG19 |
| 5877364 | EC | | 89.65 | GG19 |
| 6042191 | EC | 4986 | 43.39 | GG19 |
| 6286155 | EC | 5062 | 14.54 | GG19 |
| 6525209 | EC | 5207 | 75.13 | GG19 |
| 6850665 | EC | 4828 | 214.72 | GG19 |
| 8129189 | EC | 5080 | 53.65 | GG19 |
| 8143170 | EC | 4957 | 28.79 | GG19 |
| 8308347 | EC | 4826 | 164.95 | GG19 |
| 8564976 | EC | 4726 | 152.83 | GG19 |
| 9181877 | EC | 4599 | 0.32 | GG19 |
| 10485250 | EC | 4957 | 16.47 | GG19 |
| 10491544 | EC | 4835 | 22.77 | GG19 |
| 10920813 | EC | | 53.74 | GG19 |
| 11135978 | EC | 5004 | 0.29 | GG19 |
| 11768970 | EC | 5038 | 15.54 | GG19 |
| 12367310 | EC | 4965 | 8.63 | GG19 |
| 6042423 | HB | 4689 | | ($\nu_{\max} > 100$) B15b |
| 10188415 | HB | | | ($\nu_{\max} > 100$) B15b |
| 10322133 | HB | 5223 | | ($\nu_{\max} > 100$) B15b |

Table B.1. Catalogue and parameters for oscillating red-giant binaries characterized through photometry from the TESS mission. (The full version of the table is available in the electronic version of the paper.)

| SB9 Seq | TIC | TESS Sectors | V [mag] | T_{eff} [K] | ν_{max} [μHz] | $\Delta\nu$ [μHz] | M [M_{\odot}] | R [R_{\odot}] | logg [dex] | P_{orbit} [days] | e | K_1 [km/s] | K_2 [km/s] | SB9 Grade |
|------------|-----------|-----------------|------------|-------------------------|--|-----------------------------------|----------------------|----------------------|---------------|------------------------------|-----------------|-----------------|-----------------|--------------|
| 2882 | 49243933 | 3 | 6.87 | 5000 ± 150 | 2.13 | 0.38 | 3.3 | 72.4 | 1.25 | 1509.6 ± 1 | 0.658 ± 0.1 | 6.27 | — | — |
| 2954 | 243337598 | 9 | 5.91 | 5000 ± 151 | 2.84 | 0.5 | 2.7 | 56.2 | 1.37 | 3856 ± 22 | 0.57 ± 0.01 | 4.1 | — | — |
| 3869 | 86279245 | 2 | 6.23 | 5000 ± 152 | 3.15 | 0.6 | 1.8 | 43.8 | 1.42 | 184.258 ± 0.023 | 0.102 ± 0.008 | 8.34 | — | 5 |
| 3901 | 233829187 | 2 | 9.68 | 5000 ± 153 | 3.94 | 0.71 | 1.8 | 39.2 | 1.51 | 541 ± 0.8 | 0.043 ± 0.012 | 6.37 | — | 5 |
| 1864 | 302537716 | 2 | 10.10 | 5000 ± 154 | 5.42 | 0.9 | 1.8 | 33.5 | 1.65 | 241.9 ± 1 | 0.04 ± 0.06 | 4.7 | — | — |
| 2155 | 237415575 | 2 | 7.12 | 5000 ± 155 | 5.59 | 0.89 | 2.1 | 35.2 | 1.66 | 1768 ± 23 | 0 | 2.58 | — | — |
| 1869 | 284428523 | 2 | 6.14 | 5000 ± 156 | 5.8 | 0.89 | 2.3 | 36.4 | 1.68 | 2230 ± 23 | 0.14 ± 0.04 | 2.77 | — | — |
| 958 | 165509120 | 2 | 8.00 | 5000 ± 157 | 6.2 | 0.98 | 1.9 | 32.3 | 1.71 | 794.5 | 0.69 | 11.5 | — | 4 |
| 1098 | 236777961 | 13 | 4.64 | 5000 ± 158 | 7.75 | 1.32 | 1.2 | 22.5 | 1.81 | 138.42 ± 0.016 | 0.114 ± 0.014 | 23.46 | — | 3 |
| 1746 | 115581508 | 3 | 6.36 | 5000 ± 159 | 9.11 | 1.52 | 1.1 | 20.0 | 1.88 | 4991 ± 17 | 0.404 ± 0.011 | 4.78 | — | 5 |
| 788 | 383477233 | 1 | 7.59 | 5000 ± 160 | 10.48 ± 0.5 | 1.39 ± 0.59 | 2.3 ± 1.9 | 26.9 ± 16.2 | 1.94 ± 0.02 | 699.3 | 0.4 | 14.9 | — | 4 |
| 2885 | 49253887 | 3 | 7.79 | 5000 ± 161 | 11.65 ± 1.6 | 1.3 ± 1.41 | 3.9 ± 8.6 | 33.5 ± 51.7 | 1.98 ± 0.06 | 1212.6 ± 2.6 | 0.575 ± 0.007 | 8.18 | — | — |
| 1568 | 161624708 | 2 | (l=5.1) | 5000 ± 162 | 11.66 ± 0.82 | 1.64 ± 0.3 | 1.7 ± 0.6 | 21.8 ± 5.9 | 1.98 ± 0.03 | 6500 | 0.645 ± 0.028 | 3.49 | — | 5 |
| 2624 | 63445000 | 2 | 7.90 | 5000 ± 163 | 13.07 ± 1.01 | 1.59 ± 0.32 | 2.6 ± 1.1 | 25.6 ± 7.6 | 2.03 ± 0.03 | 1593 ± 0.6 | 0.6561 ± 0.0021 | 18.11 | — | — |
| 950 | 85379733 | 2 | 5.07 | 5000 ± 164 | 14.01 ± 0.88 | 2.04 ± 0.21 | 1.2 ± 0.3 | 17.0 ± 2.7 | 2.06 ± 0.03 | 876.25 | 0.61 | 4.8 | — | 3 |
| 229 | 417891254 | 1 | 8.16 | 5000 ± 165 | 14.8 ± 0.66 | 2.17 ± 2.03 | 1.1 ± 2.1 | 15.9 ± 21.1 | 2.09 ± 0.02 | 488 | 0.44 | 4 | — | 3 |
| 1279 | 329613266 | 2 | 7.44 | 5000 ± 166 | 16.57 ± 1.15 | 1.75 ± 0.29 | 3.5 ± 1.2 | 26.4 ± 6.5 | 2.14 ± 0.03 | 581.4 | 0.29 | 8 | — | 3 |
| 3596 | 358152485 | 2 | 6.21 | 5000 ± 167 | 17.14 ± 3.33 | 2.27 ± 0.31 | 1.4 ± 0.6 | 16.8 ± 4.6 | 2.15 ± 0.08 | 215.3021 ± 0.0665 | 0.124 ± 0.049 | 21.69 | 20.52 | 5 |
| 393 | 438006090 | 2 | 7.64 | 5000 ± 168 | 17.68 ± 1.21 | 1.99 ± 0.68 | 2.6 ± 1.8 | 22.1 ± 10.8 | 2.16 ± 0.03 | 111.69 | 0.12 | 7.8 | — | 3 |
| 3920 | 83620534 | 3 | 6.91 | 5000 ± 169 | 18.15 ± 1.11 | 2.08 ± 0.34 | 2.4 ± 0.8 | 20.8 ± 5.0 | 2.18 ± 0.03 | 1006.9 ± 0.4 | 0.04 ± 0.005 | 8.77 | — | 5 |
| 796 | 357387775 | 1 | 7.89 | 5000 ± 170 | 18.65 ± 1.03 | 2.44 ± 0.42 | 1.4 ± 0.5 | 15.8 ± 4.0 | 2.19 ± 0.03 | 302.67 | 0.49 | 8.6 | — | 4 |
| 1238 | 290519412 | 1 | 6.08 | 5000 ± 171 | 19.2 ± 2.0 | 2.32 ± 0.19 | 1.8 ± 0.4 | 17.8 ± 2.8 | 2.20 ± 0.04 | 117.776 | 0.24 | 22.6 | — | 4 |
| ... | ... | ... | ... | ... | ... | ... | ... | ... | ... | ... | ... | ... | ... | ... |

Notes. See Appendix B for a detailed description of each column of the table.

Table B.2. Catalogue and parameters for oscillating red-giant binaries characterized through photometry from the *Kepler* and **K2** mission.

| SB9 Seq | TIC | KIC | Q | V [mag] | T _{eff} [K] | v _{max} [μHz] | Δv [μHz] | M [M/M _⊙] | R [R/R _⊙] | logg [dex] | P _{orbit} [days] | e | K ₁ [km/s] | K ₂ [km/s] | SB9 Grd |
|------------|-----------|----------------|---|------------|-------------------------|---------------------------|-------------|--------------------------|--------------------------|---------------|------------------------------|------------------|--------------------------|--------------------------|------------|
| 3242 | 139109614 | KIC 5023931 | * | 15 | 13.32 | 4728 ± 92 (A) | 51.9 ± 1.1 | 4.88 ± 0.10 | 1.7 ± 0.1 | 10.6 ± 0.4 | 2.62 ± 0.01 | 209.89 ± 0.04 | 0.585 ± 0.007 | 20.5 | - |
| 3241 | 139154243 | KIC 5112840 | | 12 | 13.84 | 5053 ± 90 (A) | 112.1 ± 1.9 | 8.85 ± 0.35 | 1.8 ± 0.2 | 7.2 ± 0.4 | 2.97 ± 0.01 | 5200 ± 120 | 0.1 ± 0.04 | 3.44 | - |
| 3243 | 139109487 | KIC 5024240 | * | 14 | 14.32 | 4990 ± 108 (A) | 145.8 ± 2.2 | 12.05 ± 0.26 | 1.1 ± 0.1 | 5.1 ± 0.2 | 3.08 ± 0.01 | 66.837 ± 0.016 | 0.22 ± 0.03 | 4.04 | - |
| 3233 | 184011023 | KIC 5024851 | * | 15 | 11.69 | 4124 ± 68 (A) | 3.9 ± 0.7 | 0.65 ± 0.10 | 1.9 ± 0.8 | 41.8 ± 11.7 | 1.47 ± 0.07 | 2379 ± 9 | 0.24 ± 0.04 | 5.76 | - |
| 3234 | 139109185 | KIC 4937056 | * | 14 | 13.12 | 4848 ± 85 (A) | 48.3 ± 3.8 | 5.06 ± 0.09 | 1.3 ± 0.2 | 9.4 ± 0.8 | 2.59 ± 0.03 | 2920 ± 30 | 0.39 ± 0.03 | 6.01 | - |
| 3236 | 139109401 | KIC 5023953 | * | 15 | 12.94 | 4872 ± 86 (A) | 49.9 ± 2.0 | 4.68 ± 0.04 | 1.9 ± 0.1 | 11.2 ± 0.5 | 2.61 ± 0.02 | 7369 ± 19 | 0.608 ± 0.012 | 4.28 | - |
| 3237 | 139154396 | KIC 5112361 | * | 15 | 13.31 | 4813 ± 90 (A) | 66.1 ± 4.0 | 6.16 ± 0.17 | 1.4 ± 0.2 | 8.6 ± 0.6 | 2.73 ± 0.03 | 1449 ± 4 | 0.06 ± 0.03 | 5.13 | - |
| 3231 | 139109502 | KIC 5024476 | | 15 | 12.83 | 5054 ± 91 (A) | 66.4 ± 1.6 | 5.66 ± 0.13 | 2.1 ± 0.1 | 10.4 ± 0.4 | 2.74 ± 0.01 | 1524 ± 5 | 0.24 ± 0.04 | 5.37 | - |
| 3239 | 139153844 | KIC 5024414 | * | 14 | 12.95 | 5042 ± 99 (A) | 78.5 ± 3.9 | 6.36 ± 0.17 | 2.2 ± 0.2 | 9.7 ± 0.6 | 2.81 ± 0.02 | 3360 ± 50 | 0.72 ± 0.06 | 4.7 | - |
| 3247 | 184011491 | KIC 4937775 | * | 8 | 13.45 | 5093 ± 164 | 89.2 ± 7.7 | 7.36 ± 0.15 | 1.9 ± 0.3 | 8.3 ± 0.8 | 2.87 ± 0.04 | 1240 ± 30 | 0.35 ± 0.06 | 4 | - |
| 3246 | 139153963 | KIC 5024582 | * | 14 | 13.01 | 4803 (A) | 47.2 ± 4.3 | 5.00 ± 0.29 | 1.2 ± 0.2 | 9.3 ± 1.1 | 2.58 ± 0.04 | 1584 ± 10 | 0.39 ± 0.06 | 3.94 | - |
| 3101 | 405717854 | KIC 11753949 | | 14 | 6.43 | 4336 ± 71 (A) | 11.3 ± 1.5 | 1.65 ± 0.19 | 1.2 ± 0.4 | 19.4 ± 4.1 | 1.94 ± 0.05 | 674.7 ± 0.5 | 0.022 ± 0.004 | 7.81 | - |
| 3515 | 27186427 | KIC 11408263 | | 18 | 6.46 | 4840 ± 74 | 41.8 ± 4.5 | 4.52 ± 0.57 | 1.3 ± 0.4 | 10.2 ± 2.1 | 2.53 ± 0.04 | 4204 ± 100 | 0.3898 ± 0.0086 | 4.7 | - |
| 2660 | 63289148 | KIC 9528112 | | 17 | 7.18 | 3313 ± 144 | 28.8 ± 2.9 | 3.43 ± 0.08 | 0.7 ± 0.1 | 10.1 ± 1.1 | 2.29 ± 0.04 | 926.3 ± 36.4 | 0.08 ± 0.2 | 1.8 | - |
| 3235 | 139153978 | KIC 5112741 | g | 17 | 12.76 | 4877 ± 72 | | | | | | 17.6978 ± 0.0003 | 0.022 ± 0.012 | 42.7 | - |
| 1151 | 350739215 | KIC 11913210 | g | 3 | 7.08 | 3709 ± 366 | | | | | | 5750 | 0.29 | 6.8 | 2 |
| 1827 | 437039582 | EPIC 211394348 | | 1 | 12.03 | 4930 ± 82 | 119.0 ± 6.0 | 9.90 ± 0.95 | 1.3 ± 0.3 | 6.1 ± 0.9 | 2.99 ± 0.02 | 1233 ± 19 | 0.13 ± 0.05 | 4.4 | - |
| 1925 | 175290697 | EPIC 211976270 | | 2 | 6.92 | 5040 ± 54 | 76.0 ± 7.0 | 6.57 ± 0.34 | 1.8 ± 0.3 | 8.8 ± 1.0 | 2.80 ± 0.04 | 994.4 ± 1.2 | 0.806 ± 0.004 | 9.8 | - |
| 2586 | 14602163 | EPIC 211993818 | | 2 | 7.38 | 5716 ± 72 | 60.0 ± 7.0 | 5.81 ± 2.87 | 1.8 ± 1.8 | 9.6 ± 6.8 | 2.72 ± 0.05 | 3900 ± 17 | 0.61 ± 0.007 | 18.75 | - |

Notes. See Appendix B for a detailed description of each column of the table. *Q* gives the numbers of Quarters of *Kepler* data were obtained. Two flags are used to indicate special characteristics of the systems, described in the paper. Systems which are confirmed members of NGC 6819 are indicated with a flag ‘**’ besides the KIC identifier. The label ‘g’ stands for non-oscillating stars, which were confirmed to be giants from their clear granulation signature in the PSD of *Kepler* data. The star that falls into the described red-giant desert are marked through the flag ‘***’. Temperatures which are taken from the Apogee catalogue are flagged with an (A).

Table B.3. Literature values for system seismically characterized from BRITe photometry or radial-velocity studies.

| SB9 Seq | HD | Alt.ID | Instrument | V [mag] | T _{eff} [K] | Seismic diagnostic | P _{rot} [d] | M [M/M _⊙] | R [R/R _⊙] | logg [dex] | P _{orbit} [days] | e | K ₁ [km/s] | Reference |
|------------|--------|--------------------|------------|------------|-------------------------|----------------------------------|---|--------------------------|--------------------------|----------------|------------------------------|---------------|--------------------------|-----------|
| 2837 | 194317 | 39 Cyg | BRITe/UBr | 19d | 4.44 | v _{max} = 9.4 ± 0.7 μHz | - 1.9 ± 0.1 | 1.9 ± 0.1 | 1.9 ± 0.1 | 1.91 ± 0.02 | 31292 ± 324 | 0.495 ± 0.023 | 3.23 | K19 |
| 3489 | 101379 | 12 Mus | BRITe/BHR | 152d | 5.1 | τ _{ACF} = 5252 min | - 1.0 ± 0.3 | 16.6 ± 1 | 1.96 ± 0.03 | 61.408 ± 0.027 | 0.012 ± 0.01 | 0.012 ± 0.01 | 12.91 | K19 |
| 2601 | 28307 | θ ¹ Tau | RV (MSC) | 190d | 3.84 | 5000 ± 150 | v _{max} ≈ 90 μHz, Δv = 6.9 ± 0.2 | 138.2 | ~2.7 | ~10 | 5939 ± 46 | 0.57 ± 0.022 | 7.17 | B15a |

Notes. See Section B for more details on the columns of the table. In addition to the content described, the third column reports a more commonly known catalogue identifier. The last two columns report on the observational technique, and the analysis method. BRITe indicates photometric observations with the BRITe satellite. MSC-RV stands for multi-site campaign to measure the radial-velocity variations. While 39 Cyg and θ¹ Tau exhibited significant oscillation mode amplitudes, which allowed the direct measurement of v_{max} through a multicomponent fit, the seismic inferences were drawn from the granulation signal. K19: Kallinger et al. (2019), B15a: Beck et al. (2015b)

Table B.4. Catalogue and parameters for red-giant binaries characterized through photometry from the *Kepler* and *K2* mission for which no signature of oscillations were detected.

| SB9 Seq | TIC | KIC | Obs | V [mag] | T _{eff} [K] | P _{orbit} [days] | e | K ₁ [km/s] | K ₂ [km/s] | SB9 Grade |
|------------|-----------|----------------|-----|------------|-------------------------|------------------------------|---------------|--------------------------|--------------------------|--------------|
| 3244 | 138970759 | KIC 5023822 | 14 | 14.97 | | 40.744 ± 0.008 | 0.586 ± 0.009 | 14.21 | — | — |
| 3248 | 139109639 | KIC 5024150 | 5 | 14.5 | | 7810 ± 60 | 0.67 ± 0.04 | 3.8 | — | — |
| 3277 | 139109632 | KIC 5024607 | 11 | 15.23 | 4750.0 | 414 ± 3 | 0.71 ± 0.08 | 13 | — | — |
| 3264 | 184011237 | KIC 5024870 | 11 | 14.77 | | 121.57 ± 0.017 | 0.454 ± 0.008 | 15.6 | — | — |
| 3313 | 138970211 | KIC 5111815 | 14 | 15.11 | | 3.5749 | 0.01 ± 0.005 | 76.3 | 97.3 | — |
| 3310 | 139154299 | KIC 5112816 | 14 | 14.56 | | 33.2393 ± 0.0022 | 0.366 ± 0.006 | 39.97 | — | — |
| 3278 | 184010246 | KIC 5200656 | 14 | 15.2 | | 370.3 ± 2.1 | 0.11 ± 0.04 | 12.8 | — | — |
| 3258 | 184090973 | KIC 5201088 | 14 | 14.52 | 6000 | 135 ± 0.3 | 0.28 ± 0.03 | 10.3 | — | — |
| 2660 | 63289148 | KIC 9528112 | 17 | 7.18 | | 926.3 ± 36.4 | 0.08 ± 0.2 | 1.8 | — | — |
| 525 | 307679747 | EPIC 212173112 | 2 | 10.8 | | 10.173 | 0 | 32.2 | — | 1 |
| 2586 | 14602163 | EPIC 211993818 | 2 | 7.38 | | 3900 ± 17 | 0.61 ± 0.007 | 18.75 | — | — |
| 1813 | 437039105 | EPIC 211409376 | 3 | 12.57 | | 10.0552 ± 0.0001 | 0 | 52.1 | 59.4 | — |
| 1830 | 437034592 | EPIC 211385284 | 1 | 8.82 | 4750 | 1315 ± 5 | 0.15 ± 0.04 | 4.39 | — | — |
| 1833 | 46305337 | EPIC 211427165 | 3 | 13.74 | 5500 | 2.8231 ± 0 | 0 | 60.6 | 86.2 | — |
| 2957 | 188509972 | EPIC 206012818 | 1 | 7.78 | 3900 | 791.8 ± 1.1 | 0.17 ± 0.04 | 6.6 | — | — |

Notes. See Appendix B for a detailed description of each column of the table.